OPEN ACCESS
CellPress

Cell Reports
Report

Recurrent Somatic Structural Variations Contribute to Tumorigenesis in Pediatric Osteosarcoma

Xiang Chen,[1,12] Armita Bahrami,[2,12] Alberto Pappo,[3] John Easton,[1] James Dalton,[2] Erin Hedlund,[1] David Ellison,[2] Sheila Shurtleff,[2] Gang Wu,[1] Lei Wei,[1] Matthew Parker,[1] Michael Rusch,[1] Panduka Nagahawatte,[1] Jianrong Wu,[4] Shenghua Mao,[4] Kristy Boggs,[1] Heather Mulder,[1] Donald Yergeau,[1] Charles Lu,[6] Li Ding,[6] Michael Edmonson,[1] Chunxu Qu,[1] Jianmin Wang,[1] Yongjin Li,[1] Fariba Navid,[3] Najat C. Daw,[5] Elaine R. Mardis,[6,7,8] Richard K. Wilson,[6,7,9] James R. Downing,[3] Jinghui Zhang,[1,*] and Michael A. Dyer,[10,11,*] for the St. Jude Children's Research Hospital–Washington University Pediatric Cancer Genome Project

[1]Department of Computational Biology
[2]Department of Pathology
[3]Department of Oncology
[4]Department of Biostatistics
St. Jude Children's Research Hospital, Memphis, TN 38105, USA
[5]University of Texas MD Anderson Cancer Center, Houston, TX 77030, USA
[6]The Genome Institute
[7]Department of Genetics
[8]Department of Medicine
[9]Siteman Cancer Center
Washington University School of Medicine in St. Louis, St. Louis, MO 63108, USA
[10]Department of Developmental Neurobiology, St. Jude Children's Research Hospital, Memphis, TN 38105, USA
[11]Howard Hughes Medical Institute, Chevy Chase, MD 20815, USA
[12]These authors contributed equally to this work
*Correspondence: jinghui.zhang@stjude.org (J.Z.), michael.dyer@stjude.org (M.A.D.)
http://dx.doi.org/10.1016/j.celrep.2014.03.003

SUMMARY

Pediatric osteosarcoma is characterized by multiple somatic chromosomal lesions, including structural variations (SVs) and copy number alterations (CNAs). To define the landscape of somatic mutations in pediatric osteosarcoma, we performed whole-genome sequencing of DNA from 20 osteosarcoma tumor samples and matched normal tissue in a discovery cohort, as well as 14 samples in a validation cohort. Single-nucleotide variations (SNVs) exhibited a pattern of localized hypermutation called kataegis in 50% of the tumors. We identified p53 pathway lesions in all tumors in the discovery cohort, nine of which were translocations in the first intron of the *TP53* gene. Beyond *TP53*, the *RB1*, *ATRX*, and *DLG2* genes showed recurrent somatic alterations in 29%–53% of the tumors. These data highlight the power of whole-genome sequencing for identifying recurrent somatic alterations in cancer genomes that may be missed using other methods.

INTRODUCTION

Osteosarcoma is the most common malignant bone tumor in children and adolescents, with approximately 400 new cases each year in the United States (Ottaviani and Jaffe, 2009). Although most cases are sporadic, the risk of osteosarcoma is increased in patients with various genetic diseases, including hereditary retinoblastoma, Li Fraumeni syndrome, and germline mutations of *RecQL4* (Hicks et al., 2007; Kleinerman et al., 2005; McIntyre et al., 1994). Current multimodal therapies that incorporate surgical excision and combination chemotherapy (i.e., doxorubicin, methotrexate, and cisplatin) cure approximately 70% of patients (Meyers et al., 2005). However, clinical outcomes and therapeutic strategies have remained virtually unchanged over the past 20 years (Smith et al., 2010).

In this study, we characterized the genomic landscape of osteosarcoma by performing whole-genome sequencing (WGS) on 34 osteosarcoma tumor and matched nontumor tissue samples from 32 patients. Our results demonstrate that pediatric osteosarcomas have one of the highest rates of SVs of any pediatric cancer sequenced to date (Downing et al., 2012), but relatively few recurrent single-nucleotide variations (SNVs). However, when SVs and SNVs were combined, inactivating mutations were identified in several cancer pathways. Taken together, our results provide insights into the molecular pathology of pediatric osteosarcoma and demonstrate that comprehensive WGS is required to elucidate the complete genetic landscape of osteosarcoma.

RESULTS

WGS of Primary and Metastatic Osteosarcomas

Using a paired-end sequencing approach, we generated 10,265 Gb of sequence data for DNA in 20 osteosarcomas and matched

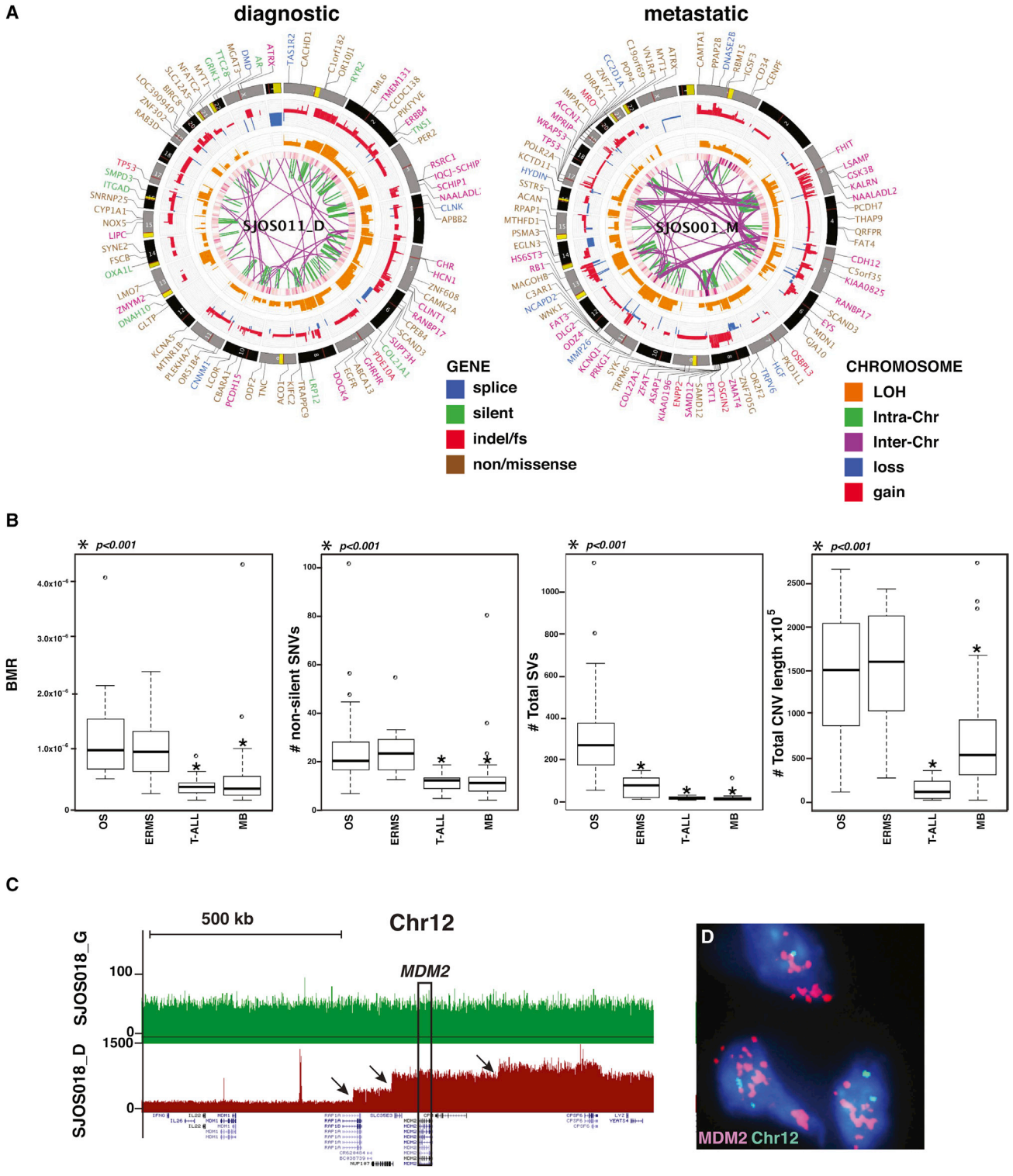

Figure 1. WGS of Osteosarcoma

(A) Representative CIRCOS plots of validated mutations and chromosomal lesions in diagnostic and metastatic osteosarcoma tumors from different patients. LOH (orange), gain (red), and loss (blue) are shown. Intrachromosomal (green lines) and interchromosomal (purple lines) translocations are indicated. Sequence mutations in RefSeq genes included silent SNVs (green), nonsense and missense SNVs (brown), splice-site mutations (dark blue), and insertion/deletion mutations (red). An additional track was added to the innermost ring of the plot showing the density of SNVs to highlight regions adjacent to SVs characteristic of kataegis.

(legend continued on next page)

normal DNA from 19 osteosarcoma patients in a discovery cohort, and 14 tumor specimens and matched normal DNA from 13 patients in a validation cohort (Table S1); 9,671 Gb (94%) were successfully mapped to the reference genome (Table S2). In the discovery cohort, the samples included 17 pre-treatment diagnostic samples (16 primary and one metastatic), one recurrent metastatic sample (SJOS001), and two tumor specimens (SJOS010_D and SJOS010_M) from the same patient with metachronous osteosarcoma (Table S1).

The average genome coverage was 44× and the average exon coverage was 39×; 99% of SNPs detected across all 39 genomes showed concordance with their corresponding SNP array genotype calls (Table S2). Validation was carried out using custom liquid capture for all SNVs, SVs, and insertions or deletions (indels) identified in the original sequence data. Combining the discovery and validation cohorts, we identified 50,426 validated somatic sequence mutations and 10,806 SVs (Table S3). These included 856 nonsilent tier 1 mutations in genes, 4,651 tier 2 mutations in evolutionarily conserved regions of the genome, and 43,782 tier 3 mutations in nonrepetitive regions of the genome that are not part of tier 1 or tier 2 (Table S3). The average number of sequence mutations was 1,483.1 per case (range 610–5,178), with 25.2 mutations per case (range 5–103) resulting in amino acid changes (Table S3). The estimated mean mutation rate was 1.15×10^{-6} per base (range 4.90×10^{-7}–3.99×10^{-6}). Among the validated SVs, 377 were predicted to produce an in-frame fusion protein (Table S3). Good-quality RNA sequencing (RNA-seq) data were available for five tumors with 64 predicted fusion SVs. Among them, 15 SVs (23%) were expressed (Table S3).

Primary and metastatic osteosarcomas had high rates of validated SVs (Figures 1A and S1). The number of SVs and CNVs, background mutation rate, and number of nonsilent tier 1 mutations were significantly higher in osteosarcoma compared with medulloblastoma and T-ALL (Robinson et al., 2012; Zhang et al., 2012; Figure 1B). However, only the number of SVs was significantly higher in osteosarcoma compared with another pediatric solid tumor with high rates of somatic alterations (embryonal rhabdomyosarcoma) (Chen et al., 2013; Figure 1B). The global patterns revealed by the WGS analysis of osteosarcoma suggest that the majority of SVs and CNVs were generated by sequential accumulation of SVs (Figures 1C and 1D), but chromothripsis (Stephens et al., 2011) was detected at specific genomic regions in four samples (chr14 in SJOS002_D, chr17q in SJOS003_D, chr6q in SJOS005_D, and chr13 in SJOS010_M; Supplemental Experimental Procedures). We used a modified version of GISTIC analysis to identify regions of the osteosarcoma genome with recurrent copy number alterations in the discovery cohort. The *TP53*, *RB1*, *MYC*, and *PTEN* pathways, as well as *ATRX*, *LSAMP-AS3*, *CCNE1*, and a genomic region on chromosome 16 containing *COPS3*, *PMP22*, *MAPK7*, *NCOR1*, and *UBB*, were recurrently mutated (Figure S1C). Among SNVs with sufficient coverage in both SJOS010 samples (20×), we validated 673 SNVs in both samples, 1,686 in diagnostic-only samples, and 1,408 in metastasis-only samples, indicating that these two tumors shared a limited amount of common mutations and were divergent early in the progression.

Applying the GRIN method (Pounds et al., 2013) on functional mutations (including SNVs and indels) and SVs, we identified *TP53* (false discovery rate [FDR] = 3.6E-51, mutated in 28/34 samples) *RB1* (FDR = 1.1E-5, mutated in 10/34 samples), *ATRX* (FDR = 2.4E-4, mutated in 10/34 samples), and *DLG2* (FDR = 0.044, mutated in 18/34 samples) as significantly mutated genes. All genes except *DLG2* were mutated by point mutations (nine for *TP53*, three for *RB1*, and five for *ATRX*) and SVs in multiple tumors (18 for *TP53*, seven for *RB1*, and five for *ATRX*). *DLG2* was exclusively mutated by SVs.

Osteosarcoma Tumor Purity and Tumor Heterogeneity

Using the purity-adjusted mutant allele fraction (MAF) derived from deep sequencing of all SNVs by capture enrichment and Illumina sequencing, we analyzed intratumor heterogeneity. Eleven tumors (SJOS001_M, SJOS004, SJOS005, SJOS008, SJOS012, SJOS013, SJOS015, SJOS001103_D1, SJOS001105_D1, and SJOS001123_D1, and SJOS001125_D1) were excluded from quantitative heterogeneity analysis due to an insufficient number of SNVs in copy-neutral regions. Statistical modeling demonstrated that 61% (14/23) of osteosarcomas in this group had evidence of multiple clones, including metastatic samples SJOS010_M, SJOS001107_M1 and SJOS001107_M2 (Figure S2).

Kataegis in Osteosarcoma

To determine whether there was any relationship between the SVs and location, distribution, or type of SNV in the osteosarcoma genomes, we plotted the validated SVs and SNVs for each sample and analyzed the intermutation distance (Figure S2). Hypermutable regions with the five hallmarks of kataegis (Nik-Zainal et al., 2012) were identified in 17 of the osteosarcoma tumors (Figure 2A). These five hallmarks of kataegis are (1) enriched C->T and C->G substitutions at TpCpX trinucleotides (Figures 2B and 2C), (2) the same class of nucleotide mutation occurring for contiguous stretches before switching to a different class (Figure 2D), (3) mutations within short stretches of the genome occurring on the same parental chromosome (Figure S2), (4) clustering of heavily mutated short stretches of the genome at multiple scales (Figure 2E), and (5) association of the hypermutated region with SV breakpoints (Figure 2E). The regions of the genome with kataegis were not recurrent in our cohort and were not associated with recurrently mutated genes

(B) Boxplots of validated basal mutation rate (BMR) and numbers of nonsilent SNVs, total SVs, and total CNVs in embryonal rhabdomyosarcoma (ERMS) and alveolar rhabdomyosarcoma (ARMS) tumors in the discovery cohort. * represents statistical significance of $p < 0.001$ as compared with the osteosarcoma genomes.

(C) Representative plot of sequence reads on chromosome 12 for the matched germline (green) and tumor (red) sample. Several distinct regions of copy number change are identified (arrows) spanning the *MDM2* gene consistent with sequential chromosomal lesions.

(D) MDM2 FISH of SJOSO18 showing amplification (red) relative to the probe for chromosome 12 (green). T-ALL, T cell acute lymphoblastic leukemia; MB, medulloblastoma.

See also Figures S1–S3 and Tables S1–S3.

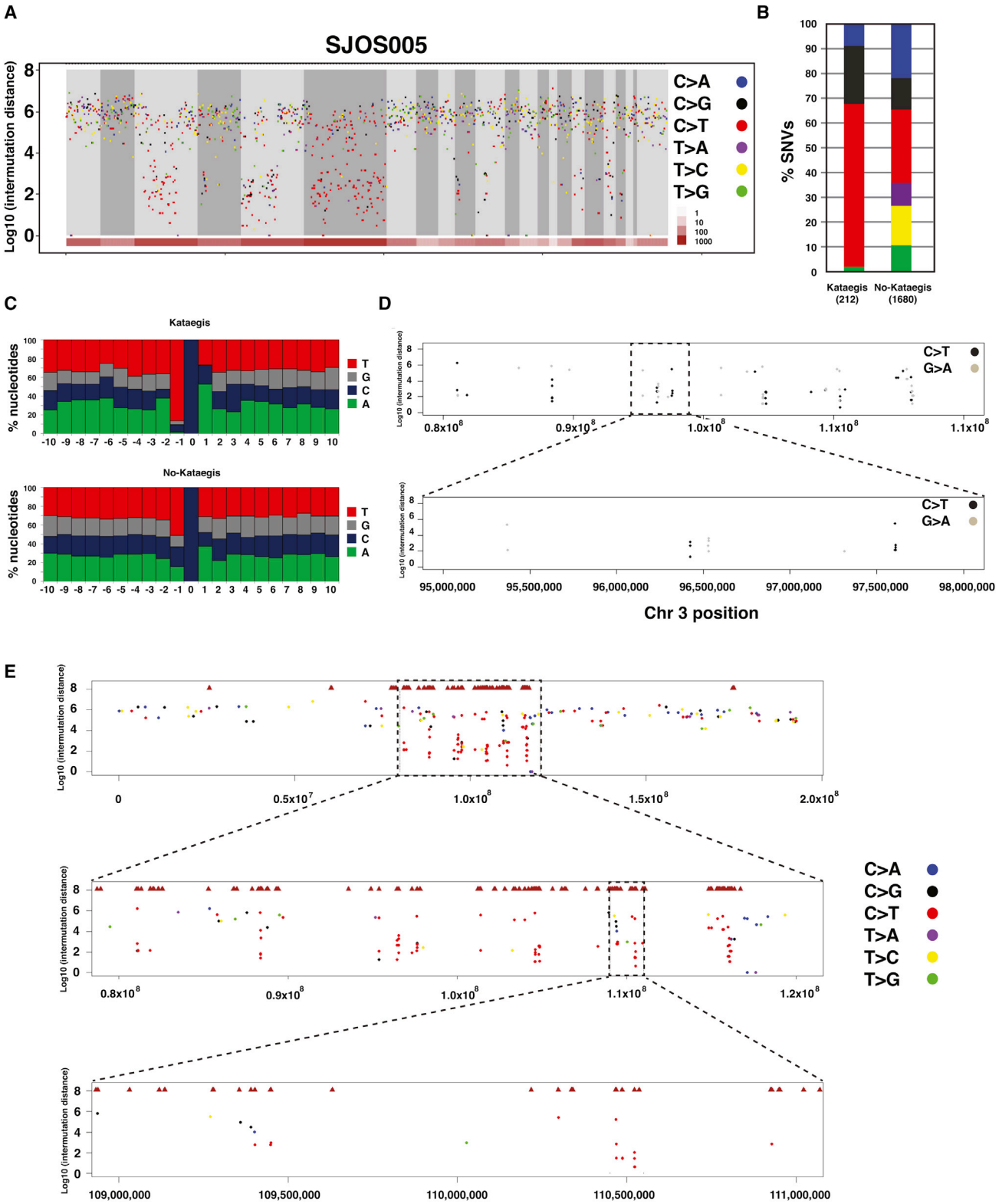

Figure 2. Kataegis in Osteosarcoma

(A) Rainfall plot showing the Log_{10} of the intermutation distance versus genomic position for a representative osteosarcoma sample (SJOS005) with evidence of kataegis. The chromosomes are demarcated by gray shading and the number of SVs in each chromosome is shown in brown at the bottom. The validated SNVs are plotted and color-coded by the type of mutation.

(legend continued on next page)

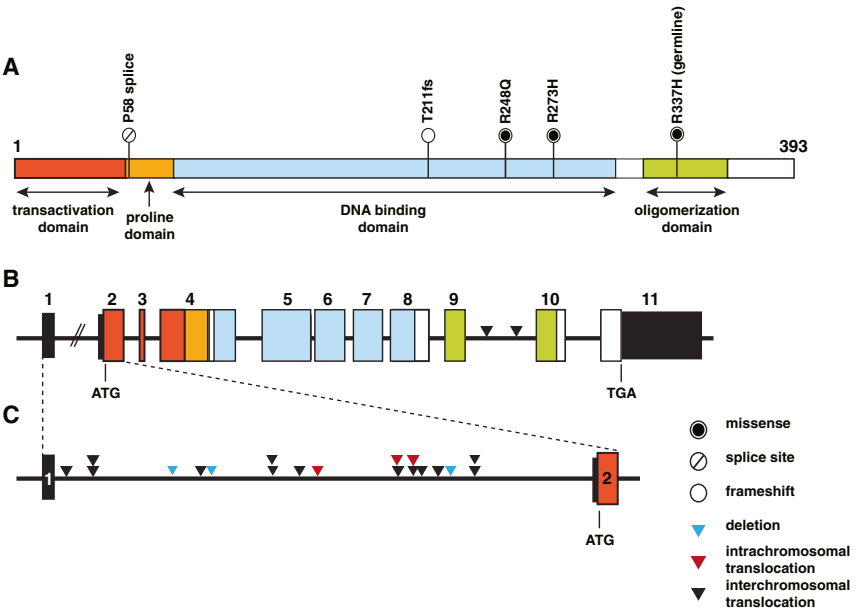

Figure 3. Validated Mutations in *TP53*

(A) Structure of the *TP53* gene showing the transactivation, proline, DNA binding, and oligomerization domains with splice-site, frameshift, and missense mutations in tumors of the 19 patients in the discovery cohort.

(B) Structure of the genomic locus of the *TP53* gene showing the exon boundaries color-coded in accordance with the protein domains shown in (A). Sites of interchromosomal translocations are indicated by black arrowheads between exons 9 and 10. The sizes of the introns and exons are scaled proportionally except for intron 1, which is much larger than the other introns in human *TP53*.

(C) A magnified view of intron 1 of *TP53* showing the deletions (blue arrowheads), intrachromosomal translocations (red arrowheads), and interchromosomal translocations (black arrowheads).

See also Figure S3 and Table S4.

in osteosarcoma (Figure S2). Tier 1 SNVs in kataegis regions were not significantly associated with the expression status ($p = 0.16$ by Fisher's exact test).

Chronology of Kataegis, SVs, and Aneuploidy in SJOS005

SJOS005 had the highest proportion (11%) of kataegis SNVs in our cohort. The large number of kataegis SNVs (n = 212) coupled with the accurate measurement of the MAFs of all SNVs derived from deep sequencing allowed us to analyze the chronology of kataegis in relation to other mutational events in this tumor. First, we examined MAFs of SNVs in kataegis microclusters containing five or more consecutive kataegis SNVs within 10 kb. The MAF variance was relatively small (6.7% of overall variance) within a microcluster, although there was a wide range of MAFs across microclusters (range 0.142–0.839, median 0.364; Figure S2). This pattern, along with the observation that SNVs in a microcluster occurred on the same parental chromosome, supports the hypothesis that SNVs in a kataegis microcluster originated from a single event. MAF analysis of SVs flanking "kataegis" clusters (range 0.132–0.866, median 0.396) also showed a significant positive correlation ($p = 4.56E-5$) with those of "kataegis" SNVs, and there was no significant difference between them ($p = 0.143$ by Wilcoxon signed rank test), indicating that the neighboring SVs likely arise simultaneously with kataegis SNVs (Figure S2).

SJOS005, like most osteosarcomas, exhibits aneuploidy with copy number gains spanning more than 50% of the genome. Kataegis SNVs were significantly enriched in regions of the genome with four or more copies compared with nonkataegis SNVs ($p < 2.2e-16$ by Fisher's exact test; Figure S2). However, the MAF distribution of kataegis SNVs showed a large fraction of SNVs with multiple copies of the mutant allele in amplified regions, whereas only a single copy of mutant alleles was found in the majority of the nonkataegis SNVs (Figure S2). Taken together, these data suggest that kataegis likely occurs before global aneuploidy, and nonkataegis SNVs occur primarily after the aneuploidy.

SVs in *TP53*

The p53 pathway was mutated in all 20 tumor samples from the 19 patients in our discovery cohort. The majority (95%, 19/20) had either sequence mutations or SVs in the *TP53* gene, and one (SJOS018) had an *MDM2* amplification (see Figures 1C and 1D; Table S3). Surprisingly, 55% of the tumors (11/20) had SVs in the *TP53* gene, and the majority of those were translocations with breakpoints that were confined to the first intron of the gene (90%, 19/21 SV breakpoints; Figures 3A–3C; Table S4). Indeed, some tumors had rearrangements in both alleles of *TP53*, resulting from two or more independent translocations (Table S4). One patient's tumor (SJOS006) had a germline SNV (R337H), one (SJOS012) had a somatic splice-site mutation, and two (SJOS004 and SJOS010) had somatic missense SNVs (Figures 3A–3C; Table S4). The remaining four patients had tumors that harbored indels in the *TP53* gene. Loss of heterozygosity (LOH) at the *TP53* locus

(B) The proportion of each type of validated SNV in osteosarcomas with evidence of kataegis versus those without kataegis.

(C) The distribution of each nucleotide sequence 5′ to the C mutations in tumors with kataegis and those without kataegis.

(D) A rainfall plot in a representative regions of chromosome 3 in SJOS005 with kataegis showing the strand of the hypermutation based on the C>T or G>A sequence clusters.

(E) A macrocluster of hypermutation with evidence of kataegis on chromosome 3 of SJOS005, with two sequential magnifications (boxes) showing the existence of microclusters within a single macrocluster.

See also Figure S2.

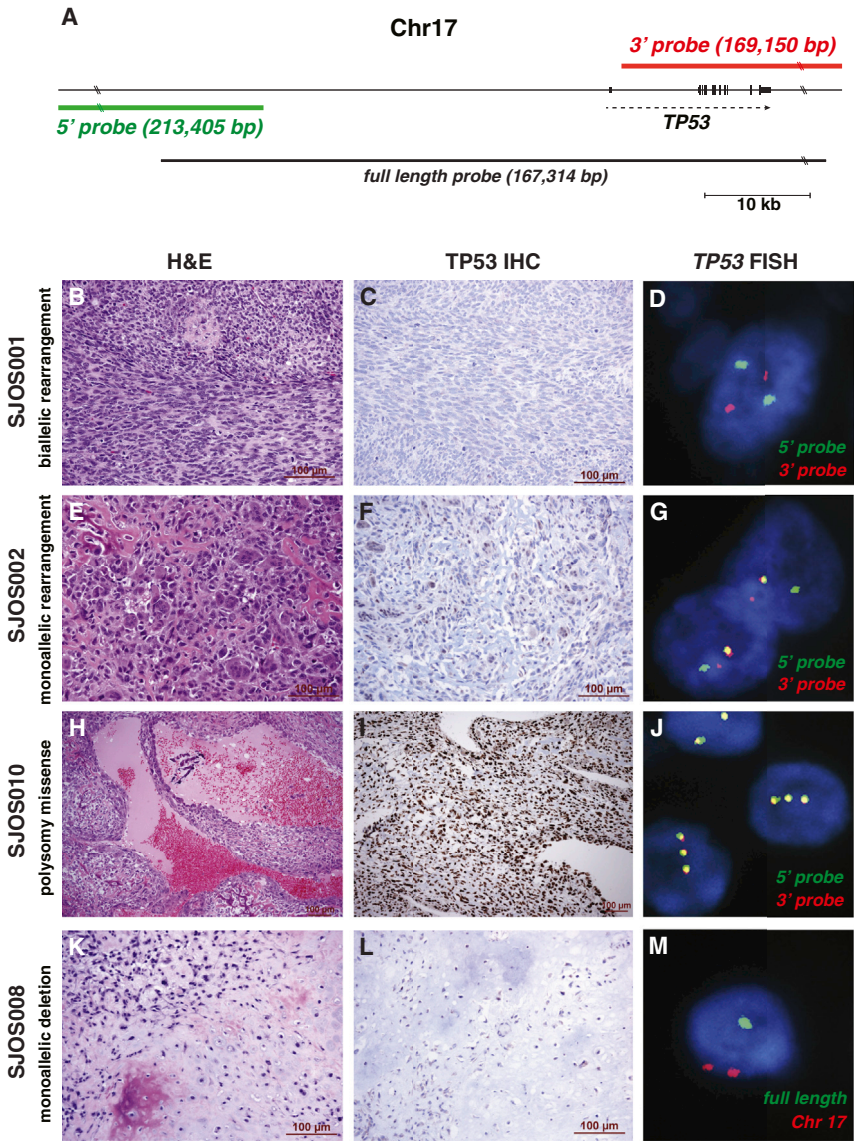

Figure 4. FISH and Immunohistochemistry for TP53 in Osteosarcoma

(A) Genomic location of the 5′ (green) and 3′ (red) break-apart FISH probes showing their position relative to the *TP53* gene. The full-length probe used to identify deletions at the *TP53* locus is shown in black.

(B–D) Images of hematoxylin and eosin (H&E), TP53 immunohistochemistry (IHC), and break-apart FISH for SJOS001 with biallelic rearrangement of the *TP53* gene.

(E–G) Images of H&E, TP53 IHC, and break-apart FISH for SJOS002 with monoallelic rearrangement of the *TP53* gene.

(H–J) Images of H&E, TP53 IHC, and break-apart FISH for SJOS010 with polysomy and a missense mutation leading to elevated accumulation of nuclear TP53 protein.

(K–M) Images of H&E, TP53 IHC, and FISH using the full-length probe (green) for SJOS008 with monoallelic deletion of *TP53*.

See also Table S5.

was evident in 40% (8/20) of the osteosarcoma tumors. In total, 15 tumors had biallelic inactivation of *TP53*, four had monoallelic inactivation of *TP53*, and one had *MDM2* amplification (Figure 1C; Table S4).

To further validate the translocations in the *TP53* gene identified by WGS, we developed a break-apart fluorescence in situ hybridization (FISH) assay with separate probes spanning the 5′ and 3′ regions of the gene (Figure 4A). We also developed a FISH assay with a probe spanning the entire *TP53* gene (Figure 4A) to assess ploidy and determine whether the gene was deleted. To complement the FISH analysis, we performed p53 immunostaining to verify that the tumors with missense mutations had accumulated high levels of nuclear p53 protein. We successfully performed FISH in 18 of 20 tumors and p53 immunostaining on all 20 tumors (Table S4). Overall, there was perfect concordance between the WGS data and the FISH data (Figures 4B–4M; Table S4).

In an additional cohort of patient tumor samples, we found that 50% (16/32) had *TP53* rearrangements, 22% (7/32) had missense mutations, 16% (5/32) had nonsense mutations, 6% (2/32) had a *TP53* deletion, and 3% (1/32) had an *MDM2* amplification (Table S5). Three patients with tumor showed no evidence of a p53 pathway mutation.

We did not find any significant difference in CNV ($p = 0.20$ by Wilcoxon rank sum test), SV ($p = 0.85$), SNV ($p = 0.43$), nonsilent tier 1 mutations ($p = 0.66$), or background mutation rate ($p = 0.43$) in the osteosarcoma samples with mutant p53 versus those with inactivating (nonsense, deletion and truncation) mutations in *TP53*. Survival analysis, including event-free survival and overall survival, did not show a significant difference in outcome for the patients whose tumors carried *TP53*-missense mutations (ten patients) versus those with *TP53*-truncating mutations (34 patients), with log rank test p values of 0.88 and 0.64, respectively.

RB1, *ATRX*, and *DLG2* Are Recurrently Mutated in Osteosarcoma

ATRX is part of a multiprotein complex that regulates chromatin remodeling, nucleosome assembly, and telomere maintenance. It was recently shown that *ATRX* mutations in neuroblastoma are associated with age at diagnosis (Cheung et al., 2012). Most neuroblastomas with *ATRX* mutations show evidence of alternative lengthening of telomeres (ALT), as measured by WGS, telomere FISH, and telomere quantitative PCR (qPCR) (Cheung et al., 2012). In our osteosarcoma discovery cohort, we identified five tumors (SJOS001, SJOS002, SJOS007, SJOS001112-M2, and SJOS001117-D1) with point mutations in *ATRX*, and five

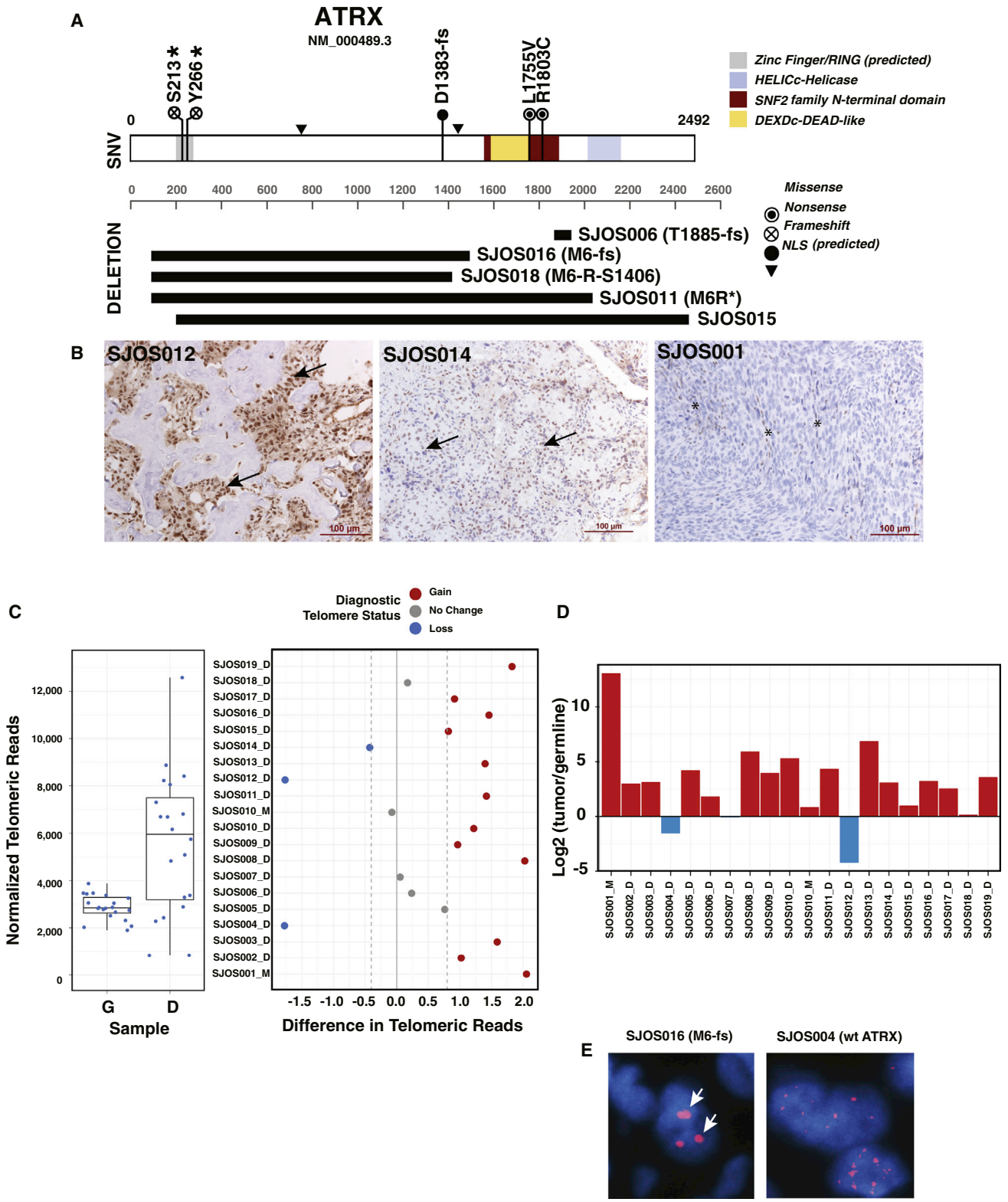

Figure 5. *ATRX* Mutations Correlate with ALT in Osteosarcoma

(A) Diagram of the five SNVs, four deletions, and one interchromosomal SV found in the *ATRX* genes of the osteosarcoma cohort. Three of the samples with ATRX SVs (SJOS006, SJOS018, and SJOS011) had matching RNA-seq data. SJ006 has a short deletion at exon 23 and the RNA-seq data confirmed a readthrough

(legend continued on next page)

with focal deletions or SVs affecting the coding region of the gene (Figure 5A; Table S6). There was no significant gender bias in *ATRX* mutations (p = 0.25 by Fisher's exact test) even though it is located on the X chromosome. By immunohistochemistry, 31% (6/19) of the tumors in the discovery cohort were ATRX negative (Figure 5B; Table S6). The sample with a missense mutation (SJOS007-R1803C) and one with an SV (SJOS018) were heterogeneous for ATRX protein expression. Analysis of telomere sequence reads from the WGS data and qPCR of telomeres showed that the majority of osteosarcomas had longer telomeres (Figures 5C and 5D), and ALT was found in 85% (12/14) of the samples using telomere FISH (Table S6).

Beyond *TP53* and *ATRX*, there were significant recurrent mutations in *RB1* (10/34, FDR *q* = 1.1E-5) and *DLG2* (18/34, FDR *q* = 0.044). *DLG2* encodes a multi-PDZ domain protein that is involved in epithelial polarity during cell division and has been implicated in cancer cell invasion. In *Drosophila*, DLG is a tumor suppressor, but a clear tumor-suppressor function has not yet been confirmed for *DLG2* in human cancer.

SVs in Cancer Genes

SVs contributed 91% (9,605/10,523) of all functional genetic lesions in our osteosarcoma cohort. In total, 122 cancer genes had at least one SV breakpoint (Table S7) and all but one tumor (SJOS001118_D1) had at least one breakpoint (range 1–40) in a cancer gene. SV breakpoint enrichment in the cancer genes was highly significant even when we excluded *TP53* from the list (p = 2.5E-6). Twelve of the 34 tumors (35%) achieved significant enrichment of SV breakpoints in cancer genes individually. In addition, some tumors have "fold-back intrachromosomal translocations" (Campbell et al., 2010) to inactivate tumor-suppressor genes (Figure S3). These results further support the hypothesis that genomic instability leads to lesions in various cancer genes.

DISCUSSION

WGS of osteosarcoma demonstrated that the rate of SNVs was similar to that in other pediatric solid tumors, and only a few recurrent SNVs were detected. Approximately half of the osteosarcomas in our discovery cohort had a pattern of hypermutation associated with SVs, called kataegis (Nik-Zainal et al., 2012). The regions of the genome with kataegis were not recurrent, and none of the most recurrently mutated genes were found in regions of kataegis. Chromosomal lesions, rather than SNVs, were the major mechanism of recurrent mutations, and many of the most significant chromosomal lesions were found in known cancer genes, including *TP53*, *RB1*, and *ATRX.*

Genomic Stability and Osteosarcoma Initiation and Progression

The most frequent mutation in osteosarcoma is in *TP53*. By our estimates, both alleles are mutated in as many as 80% of tumors, and at least one allele was mutated in >90% of tumors. These data suggest that p53 mutations are a major oncogenic driver in osteosarcoma. Although this finding is not novel, what is surprising is the mechanism of inactivation. Most *TP53* mutations are SVs in intron 1, which suggests that either the *TP53* locus is particularly susceptible to SVs or SVs occur at a high rate in the osteosarcoma tumor-initiating cell. Aside from osteosarcomas and prostate cancers (Baca et al., 2013; Berger et al., 2011), there is no evidence of *TP53* SVs in any other cancer, so the locus is probably not uniquely susceptible to chromosomal rearrangements. These data raise an intriguing possibility: genomic instability characterized by high rates of CNVs and SVs may precede *TP53* inactivation, and may be the underlying mechanism that initiates and promotes osteosarcoma.

Kataegis in Osteosarcoma

In a recent WGS study, Nik-Zainal et al. (2012) described a distinct hypermutation phenomenon in breast cancer that they termed kataegis. Here, we found SNV clusters with the same five characteristics of kataegis in 50% of the osteosarcomas analyzed by WGS. Interestingly, genomic regions encoding *TP53* and *ATRX*, the two most frequently mutated genes in osteosarcoma, did not exhibit this pattern of local hypermutation. Furthermore, there was no association between kataegis and *TP53* mutation type (i.e., SNV, indel, or SV).

TP53-Mutant or -Null Osteosarcomas

Previous studies have estimated that 20%–70% of osteosarcomas carry mutations in the p53 pathway (Lonardo et al., 1997; Wunder et al., 2005), but our data suggest that the proportion is much higher. For example, Wunder et al. (2005) sequenced exons 4–10 of the *TP53* gene in 196 osteosarcoma samples and found that 19.4% (38/196) had *TP53* SNVs. The investigators concluded that the remaining 80.6% (158/196) had wild-type *TP53* (Wunder et al., 2005). They went on to show that event-free survival was indistinguishable between the two groups (wild-type and mutant *TP53*) (Wunder et al., 2005). SVs in the first intron of *TP53* were not analyzed in that study, even though such lesions had previously been reported in osteosarcoma (Miller et al., 1990). Our data suggest that the majority of the tumors identified as *TP53* wild-type in the study

event that would result in a T1885 frameshift. For SJOS011, the RNA-seq and WGS data supported a junction connecting exon 1 to exon 28, creating a nonsense mutation (M6R*). For SJOS018, the RNA-seq and WGS data supported a deletion connecting exon 1 to exon 13, thereby creating an in-frame fusion protein (M6RS1406). The WGS for SJOS016 predicts a deletion that connects exon 1 to exon 16, producing a frameshift (M6fs).

(B) Representative IHC for ATRX showing nuclear ATRX in a sample with intense staining and wild-type ATRX (SJOS012), a sample with fainter nuclear localized ATRX (SJOS014), and a sample with a nonsense mutation (SJOS001). Arrows indicate representative nuclei stained positive for ATRX. Asterisks indicate ATRX immunopositive vascular endothelial cells among the tumor cells that are negative for ATRX IHC.

(C and D) Relative telomere length in the osteosarcomas compared with that in the matched germline DNA, as analyzed by WGS and qPCR.

(E) Representative telomere FISH showing characteristics of ALT (arrow) in an osteosarcoma with an ATRX deletion.

See also Tables S6 and S7.

by Wunder et al. (2005) actually had inactivating SVs in *TP53*. Therefore, it may be useful to revisit the association of *TP53* pathway inactivation with osteosarcoma outcome in a large cohort of patient samples.

EXPERIMENTAL PROCEDURES

Full details regarding sample acquisition, molecular and biochemical procedures, informatics, and WGS are provided in the Supplemental Information. All tumors in this study were obtained from St. Jude Children's Research Hospital (SJCRH) patients. The SJCRH IRB approved experiments involving human subjects and informed consent was obtained from all subjects.

ACCESSION NUMBERS

The European Bioinformatics Institute accession number for the sequencing data reported in this paper is EGAS00001000263.

SUPPLEMENTAL INFORMATION

Supplemental Information includes Supplemental Experimental Procedures, three figures, and seven tables and can be found with this article online at http://dx.doi.org/10.1016/j.celrep.2014.03.003.

ACKNOWLEDGMENTS

This work was supported, in part, by Cancer Center Support (CA21765) from the NCI, grants to M.A.D from the NIH (EY014867, EY018599, and CA168875), and the American Lebanese Syrian Associated Charities (ALSAC). M.A.D. is an HHMI Investigator. The whole-genome sequencing was supported as part of the St. Jude Children's Research Hospital -Washington University Pediatric Cancer Genome Project.

Received: May 10, 2013
Revised: November 22, 2013
Accepted: March 3, 2014
Published: April 3, 2014

REFERENCES

Baca, S.C., Prandi, D., Lawrence, M.S., Mosquera, J.M., Romanel, A., Drier, Y., Park, K., Kitabayashi, N., MacDonald, T.Y., Ghandi, M., et al. (2013). Punctuated evolution of prostate cancer genomes. Cell *153*, 666–677.

Berger, M.F., Lawrence, M.S., Demichelis, F., Drier, Y., Cibulskis, K., Sivachenko, A.Y., Sboner, A., Esgueva, R., Pflueger, D., Sougnez, C., et al. (2011). The genomic complexity of primary human prostate cancer. Nature *470*, 214–220.

Campbell, P.J., Yachida, S., Mudie, L.J., Stephens, P.J., Pleasance, E.D., Stebbings, L.A., Morsberger, L.A., Latimer, C., McLaren, S., Lin, M.L., et al. (2010). The patterns and dynamics of genomic instability in metastatic pancreatic cancer. Nature *467*, 1109–1113.

Chen, X., Steward, E., Shelat, A., Qu, C., Bahrami, A., Hatley, M., Wu, G., Bradley, C., McEvoy, J., Pappo, A., et al.; St. Jude Children's Research Hospital–Washington University Pediatric Cancer Genome Project (2013). Targeting oxidative stress in embryonal rhabdomyosarcoma. Cancer Cell *24*, 710–724.

Cheung, N.K., Zhang, J., Lu, C., Parker, M., Bahrami, A., Tickoo, S.K., Heguy, A., Pappo, A.S., Federico, S., Dalton, J., et al. (2012). Association of age at diagnosis and genetic mutations in patients with neuroblastoma. JAMA *307*, 1062–1071.

Downing, J.R., Wilson, R.K., Zhang, J., Mardis, E.R., Pui, C.H., Ding, L., Ley, T.J., and Evans, W.E. (2012). The Pediatric Cancer Genome Project. Nat. Genet. *44*, 619–622.

Hicks, M.J., Roth, J.R., Kozinetz, C.A., and Wang, L.L. (2007). Clinicopathologic features of osteosarcoma in patients with Rothmund-Thomson syndrome. J. Clin. Oncol. *25*, 370–375.

Kleinerman, R.A., Tucker, M.A., Tarone, R.E., Abramson, D.H., Seddon, J.M., Stovall, M., Li, F.P., and Fraumeni, J.F., Jr. (2005).). Risk of new cancers after radiotherapy in long-term survivors of retinoblastoma: an extended follow-up. J. Clin. Oncol. *23*, 2272–2279.

Lonardo, F., Ueda, T., Huvos, A.G., Healey, J., and Ladanyi, M. (1997). p53 and MDM2 alterations in osteosarcomas: correlation with clinicopathologic features and proliferative rate. Cancer *79*, 1541–1547.

McIntyre, J.F., Smith-Sorensen, B., Friend, S.H., Kassell, J., Borresen, A.L., Yan, Y.X., Russo, C., Sato, J., Barbier, N., Miser, J., et al. (1994). Germline mutations of the p53 tumor suppressor gene in children with osteosarcoma. J. Clin. Oncol. *12*, 925–930.

Meyers, P.A., Schwartz, C.L., Krailo, M., Kleinerman, E.S., Betcher, D., Bernstein, M.L., Conrad, E., Ferguson, W., Gebhardt, M., Goorin, A.M., et al. (2005). Osteosarcoma: a randomized, prospective trial of the addition of ifosfamide and/or muramyl tripeptide to cisplatin, doxorubicin, and high-dose methotrexate. J. Clin. Oncol. *23*, 2004–2011.

Miller, C.W., Aslo, A., Tsay, C., Slamon, D., Ishizaki, K., Toguchida, J., Yamamuro, T., Lampkin, B., and Koeffler, H.P. (1990). Frequency and structure of p53 rearrangements in human osteosarcoma. Cancer Res. *50*, 7950–7954.

Nik-Zainal, S., Alexandrov, L.B., Wedge, D.C., Van Loo, P., Greenman, C.D., Raine, K., Jones, D., Hinton, J., Marshall, J., Stebbings, L.A., et al.; Breast Cancer Working Group of the International Cancer Genome Consortium (2012). Mutational processes molding the genomes of 21 breast cancers. Cell *149*, 979–993.

Ottaviani, G., and Jaffe, N. (2009). The epidemiology of osteosarcoma. Cancer Treat. Res. *152*, 3–13.

Pounds, S., Cheng, C., Li, S., Liu, Z., Zhang, J., and Mullighan, C. (2013). A genomic random interval model for statistical analysis of genomic lesion data. Bioinformatics *29*, 2088–2095.

Robinson, G., Parker, M., Kranenburg, T.A., Lu, C., Chen, X., Ding, L., Phoenix, T.N., Hedlund, E., Wei, L., Zhu, X., et al. (2012). Novel mutations target distinct subgroups of medulloblastoma. Nature *488*, 43–48.

Smith, M.A., Seibel, N.L., Altekruse, S.F., Ries, L.A., Melbert, D.L., O'Leary, M., Smith, F.O., and Reaman, G.H. (2010). Outcomes for children and adolescents with cancer: challenges for the twenty-first century. J. Clin. Oncol. *28*, 2625–2634.

Stephens, P.J., Greenman, C.D., Fu, B., Yang, F., Bignell, G.R., Mudie, L.J., Pleasance, E.D., Lau, K.W., Beare, D., Stebbings, L.A., et al. (2011). Massive genomic rearrangement acquired in a single catastrophic event during cancer development. Cell *144*, 27–40.

Wunder, J.S., Gokgoz, N., Parkes, R., Bull, S.B., Eskandarian, S., Davis, A.M., Beauchamp, C.P., Conrad, E.U., Grimer, R.J., Healey, J.H., et al. (2005). TP53 mutations and outcome in osteosarcoma: a prospective, multicenter study. J. Clin. Oncol. *23*, 1483–1490.

Zhang, J., Ding, L., Holmfeldt, L., Wu, G., Heatley, S.L., Payne-Turner, D., Easton, J., Chen, X., Wang, J., Rusch, M., et al. (2012). The genetic basis of early T-cell precursor acute lymphoblastic leukaemia. Nature *481*, 157–163.